Conformational Behavior of *C*-Glycosyl Analogues of Sialyl-α-(2→3)-Galactose

Ana Poveda,[a] Juan Luis Asensio,[b] Tülay Polat,[c] Hélèn Bazin,[c] Robert J. Linhardt,[c] and Jesús Jiménez-Barbero*[b]

Keywords: C-Glycosides / Conformational analysis / Molecular dynamics / Selectins

The conformational behavior of the *C*-glycosyl analogue of sialyl-α-(2→3)-galactose, synthesized as a glycosidase inhibitor, has been studied using a combination of NMR spectroscopy (*J* and NOE data) and molecular dynamics calculations. The obtained results show that the population distribution of conformers with respect to the orientation about the pseudo-glycosidic linkages is mainly controlled by steric interactions. This is in contrast to findings made for *O*-glycosides. In these natural compounds, the conformational behavior about the glycosidic linkage Φ is mainly governed by the *exo*-anomeric effect.

Introduction

Carbohydrate–protein interactions are involved in a wide range of biological activities starting from fertilization and extending to pathological processes such as metastasis.[1,2] Since carbohydrate ligands are susceptible to hydrolytic attack, *C*-glycosides have been developed, which offer the possibility of improved chemical and biochemical stability.[3,4] However, methylene-bridged analogues do not simply behave as non-cleavable glycosides, and differences between the behaviors of *C*- and *O*-glycosides have been reported.[5] Moreover, since the substitution of an oxygen atom by a methylene group modifies both the structural parameters (1.42 Å vs. 1.55 Å for the C1–O/C1–Cb distances; 114° vs. 115° for the C1–O–C/C1–Cb–C angles) and the electronic properties of the glycosidic linkage,[6] the flexibility in the Φ/Ψ torsion angles can be markedly changed.[7] Thus, the *exo*-anomeric effect[8] due to the presence of the acetal function is no longer seen in the *C*-glycoside[9] and consequently the associated variation in the steric interactions between the residues is not seen either. Kishi and co-workers have proposed that *C*- and *O*-glycosides share the same conformational characteristics in the free state.[10,11] Moreover, the recent finding that the conformation of *C*-lactose bound to peanut agglutinin is essentially identical to that of its parent *O*-lactose bound to the same protein has elicited the claim that the conformational similarity between *O*- and *C*-glycosides is a general phenomenon.[11] In contrast, we have recently reported that similar conformations for *C*- and *O*-glycosides are not sustained in several β- and α-linked glycosides.[7a,7c,12]

This dichotomy has prompted us to study other *C*-glycosyl compounds. Among glycosides, sialyl-oligosaccharides are special compounds from a conformational point of view.[13,14] In principle, considering the three staggered conformations of the angle Φ of glycopyranosides, in the absence of additional stereoelectronic (*exo*-anomeric) effects, the orientation of the hydroxy group at the C-2 position can be expected to have a strong influence on the conformational equilibrium. For the regular $^4C_1$(D) or $^1C_4$(L) chair forms, considering the non-*exo*-anomeric (non-*exo*) conformation (Scheme 1a),[7c] a 1,3-*syn*-diaxial interaction between one equatorially substituted C-2 (*gluco* series) and the aglycon is apparent. Such steric interactions do not occur in the *exo*-anomeric *syn* and *anti* conformations (*exo-syn* and *exo-anti*). In contrast, considering the *exo*-anomeric *anti* conformation (Scheme 1b),[7c] a 1,3-type interaction can be expected between one axially substituted C-2 (*manno* series) and the aglycon. For sialic acid, the lack of a substituent at the C-3 position (equivalent to C-2 in most glycosides) means that the three staggered conformations of the angle Φ (*exo-syn*, *exo-anti*, and non-*exo*) are essentially free of interactions of this type. Furthermore, the glycosidic carbon atom of a sialyl-oligosaccharide is quaternary, which has two basic consequences with regard to the conformational behavior of these compounds. First, the presence of an electron-withdrawing COOH group at the anomeric center can be expected to increase the participation of the *exo*-anomeric effect due to the interglycosidic oxygen.[8] Second, in contrast to other glycosides, the two possible orientations of the glycosidic linkage consistent with the stereoelectronic effect (*exo-syn* and *exo-anti*) have two *gauche*-type interactions with the substituents at the anomeric center. In most glycosides, only one orientation of ϕ

[a] Servicio Interdepartamental de Investigación, Universidad Autónoma de Madrid, 28049 Cantoblanco, Spain
[b] Instituto de Química Orgánica, CSIC, Juan de la Cierva 3, 28006 Madrid, Spain
[c] Department of Chemistry, Division of Medicinal and Natural Products Chemistry and Department of Chemical and Biochemical Engineering, The University of Iowa, PHAR-S328, Iowa City, IA 52242, USA
Supporting information for this article is available on the WWW under http://www.wiley-vch.de/home/eurjoc or from the author.

  1434−193X/00/0509−1805 $ 17.50+.50/0

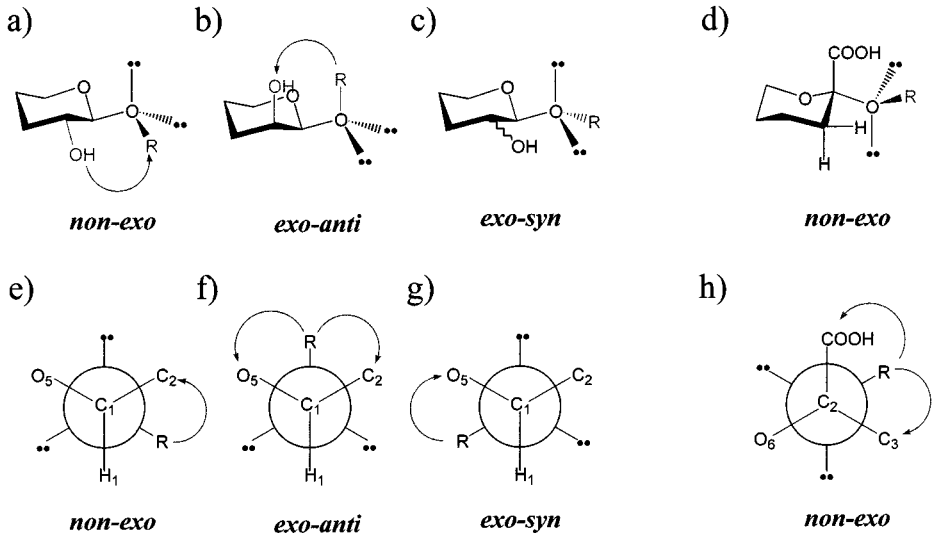

Scheme 1. (a)–(d): schematic representation of the 1,3-*syn*-diaxial-type interactions present in natural glycopyranosides (a) with an equatorial orientation of the substituent at the 2-position for a non-*exo*-anomeric orientation of the aglycon and (b) with an axial orientation of the substituent at the 2-position for an *exo-anti* orientation of the aglycon; the *exo*-anomeric *syn* orientation (c) of the aglycon is free of 1,3-*syn* diaxial interactions with 2-OH irrespective of its orientation; for sialic acid (d) the three staggered orientations about ϕ are free of these 1,3-type steric interactions; (e)–(h): schematic representation of the *gauche*-type interactions between the aglycon and the substituents at the anomeric center present in the three staggered orientations about ϕ in normal glycosides; in contrast to other glycosides, for sialic acid (h) both the *exo-syn* and *exo-anti* orientation have two *gauche*-type interactions

(*exo-syn*) is detected in solution. The *exo-anti* conformation, in which there are two *gauche*-type interactions with the vicinal substituents (Scheme 1f), is sterically destabilized with respect to the *exo-syn* form, in which there is only one *gauche*-type interaction. In sialyl-oligosaccharides, both orientations are sterically equivalent and therefore a higher degree of flexibility can be expected for the glycosidic linkages. In fact, conformational equilibria between *exo-anti* and *exo-syn* conformations, both favored by the *exo*-anomeric effect, have been reported for various sialyl-oligosaccharides.[13,14] Clearly, depending on the magnitude of the stereoelectronic effect, the energy differences between the three rotamers should be different for *C*- and *O*-glycosides, with the consequence that non-*exo*-anomeric conformers can be detected for the former compounds.

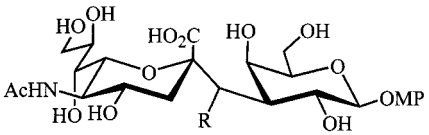

1: R = OH, (*R*) configuration
2: R = OH, (*S*) configuration

Scheme 2

The experimental investigation outlined in this paper was designed to reveal the relative importance of stereoelectronic and steric effects in sialyl-oligosaccharides and to further clarify the controversy concerning similar or dissimilar conformations of *O*-glycosides and their *C* analogues. Our primary interest in **1** (Scheme 2) stems from the hypothesis that it is a mimic of the sialyl-Gal part of sLeX, which has been shown to interact with selectins, taking part in diverse cellular activities including cell recognition and inflammatory response.[1,2,13–16] On this basis, we report here on a conformational study of *C*-α-L-sialyl-(2→3)-β-D-Gal-β-OR (**1**) by means of NMR spectroscopy and time-averaged restrained molecular dynamics (tar-MD)[17] using the AMBER force field.[18] For comparison purposes, the results obtained in several conformational studies of the parent *O*-glycoside, namely *O*-α-L-sialyl-(2→3)-β-D-Gal-β-OR (**3**), are also presented.

Results and Discussion

The *C*-glycosyl analogues of sialyl-α-(2→3)-galactose (**1** and **2**, Scheme 3) were first synthesized in their protected form[19] and then deprotected (Scheme 4) for the current study.

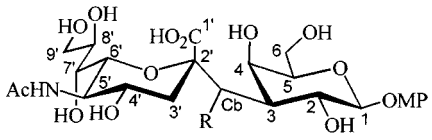

1: R = OH, (*R*) configuration
2: R = OH, (*S*) configuration

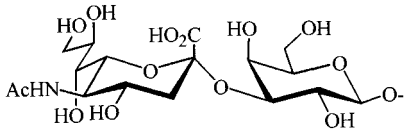

3

Scheme 3. Schematic representations of compounds **1–3**, showing the atomic numbering

Conformational Analysis

^{1}H-NMR spectra of compound **1** (Scheme 3) were assigned by standard methods using a combination of

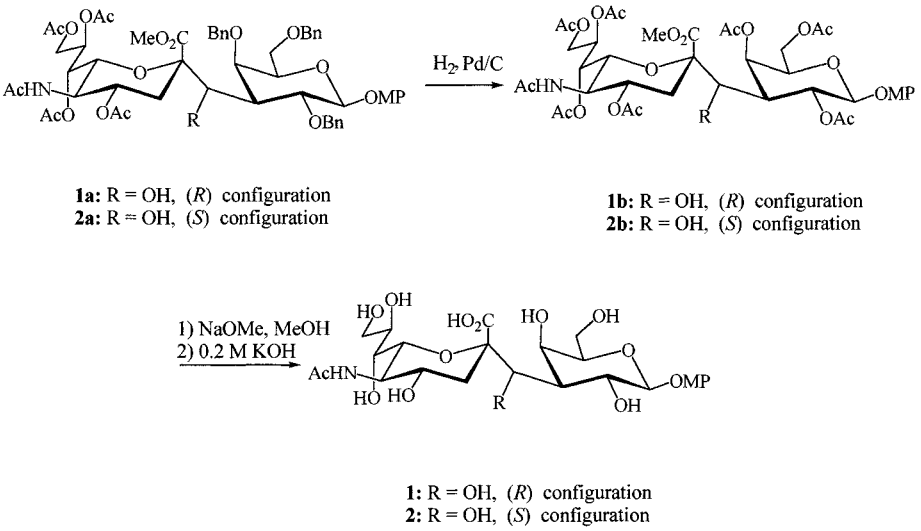

Scheme 4. Schematic representation of the method used for deprotection of compounds **1**–**2**

NOESY, TOCSY, and DQF-COSY experiments. The ^{1}H-NMR chemical shifts are given in the Supporting Information. From the collected data, it is evident that the chemical shift values strongly depend on the stereochemistry at the pseudo-glycosidic carbon atom (C_b). Assignment of the stereochemistry at C_b in **1** was achieved using a protocol similar to that described previously,[12,19] based exclusively on a combination of experimental *J*, NOE, and δ values, with additional comparison with data for the diastereomeric (*S*) analogue **2**. The glycosidic torsion angles[20–22] of **1** and **2** are defined as Φ $C1_{Sial}$–$C2_{Sial}$–C_b–$C3_{Gal}$ and Ψ $H3_{Gal}$–$C3_{Gal}$–C_b–$C2_{Sial}$. For **1**, the *exo-syn* orientation of ϕ (Scheme 5) is defined as –60°, the non-*exo* +60°, and the *exo-anti* 180°. For the Ψ angle, the *syn*(+) orientation is defined as 60°, *syn*(–) as –60°, and *anti* as 180°. From the intra-ring vicinal coupling constants,[23] it could be proved that the six-membered rings of the sialic and galactose moieties adopt $^1C_4$(L) and $^4C_1$(D) conformations, respectively. *J* values for the C7–C9 fragment of the sialic residue were essentially identical to those reported for the natural compound **3**, indicating that the preferred orientation of this chain is the same as that reported for natural sialic residues.[13–16]

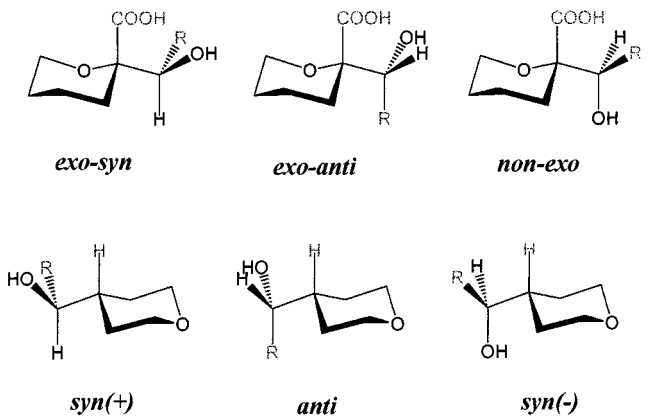

Scheme 5. Schematic representation of the three staggered orientations about Φ and Ψ of sialyl glycosides

As a first step in deducing the conformational behavior of compound **1**, potential energy surfaces were calculated using the AMBER* force field[18] (Figure 1). Two different

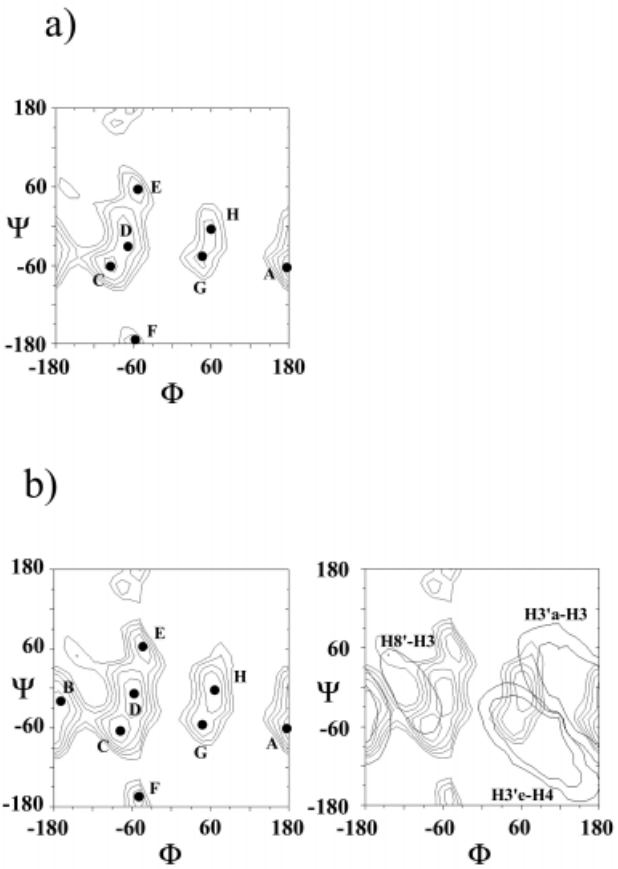

Figure 1. Steric energy maps calculated with the AMBER* forcefield with ε = 80 (a, left) and ε = 4 · *r* (b, middle); the positions of the global energy minimum (A) and the additional local minima (B–H) are marked; contours are drawn at 1 kcal mol^{-1} intervals; the expected key inter-residue NOEs are marked in the map at the right-hand side; short-distance contours are indicated at 2.5 and 3.0 Å; the corresponding maps, minima, and distances found by MM3* calculations are very similar

dielectric constant values were tested ($\varepsilon = 4^*r$ and $\varepsilon = 80$) in order to assess the effect of the electrostatic interactions on the global shape of the energy maps. The results are shown in Figure 1. These surfaces merely provide a first estimation of the conformational regions that are energetically accessible. Analysis of the maps (Table 1) reveals the presence of eight different conformational families, suggesting that these compounds are likely to be rather flexible.[15,16] Although the relative energies of the minima are to some extent dependent on the value of the dielectric constant used in the calculation, the global shapes of the two potential energy surfaces are fairly similar, indicating that the conformational equilibrium about Φ and Ψ may be extremely complicated. Thus, low-energy regions can be found for each of the staggered orientations arrived at by varying

Table 1. Torsion angle values, relative energies, and populations according to AMBER* ($\varepsilon = 4 \cdot r$ and $\varepsilon = 80$) calculations for the different minima of compound **1**

Minimum	AMBER* $\varepsilon = 4 \cdot r$			AMBER* $\varepsilon = 80$		
	Φ/Ψ (°)	ΔE	Pop. (%)	Φ/Ψ (°)	ΔE	Pop. (%)
A	174.9/–68.7	0	43.45	175.5/–67.3	0	87.56
B	–164.2/–24.0	5.0	5.92	–	–	–
C	–81.8/–68.1	3.1	34.32	–83.9/–65.8	6.0	7.93
D	–56.6/–17.2	4.3	7.84	–60.3/–3.3	9.2	2.24
E	–44.9/60.2	5.7	4.48	–44.6/58.0	10.4	1.37
F	–51.3/–167.7	11.2	0.50	–49.8/–171.1	14.7	0.24
G	45.7/–57.1	10.7	0.61	46.2/–56.8	13.7	0.37
H	62.3/6.5	6.8	2.88	63.3/3.2	14.3	0.29

the angle ϕ (Table 1): *exo-syn* (minima C, D, E, and F), *exo-anti* (minima A and B), and non-*exo* (minima G and H). The conformational behavior predicted for the angle Ψ is more complex. At each Φ region, two distinct areas can be observed in the maps: one is located around the *syn*(–) orientation (–60°), while the second is close to eclipsed (i.e. 20 ± 10°). In addition, significant minima characterized by the *syn*(+) (60°) and *anti* (180°) orientations about Ψ are present only for the *exo-syn* (–60°) orientation of the pseudo-glycosidic linkage (minima E and F, respectively). In principle, according to AMBER* calculations, two of the eight conformational families should be predominant in the equilibrium, namely the *exo-anti*/*syn*(–) (43–87%) and the *exo-syn*/*syn*(–) (8–34%). The non-*exo*/*syn*(–) family should also be present, but with a population less than 1% in all cases.

A first conformational description of the ψ aglyconic torsion of **1** was obtained on the basis of the interglycosidic vicinal proton–proton coupling constant $J_{3,b}$ and the inter-residue H–H distances that characterize these low-energy geometries. Thus, for compound **1**, the experimental value for the coupling constant $J_{3,b}$ is 1.6 Hz, ruling out the presence of significant populations of conformers characterized by the *syn*(+) orientation about ψ (for these conformers, the predicted *J* values are greater than 10 Hz due to the *trans* disposition of H_b and $H3_{Gal}$). In addition, this small value shows a better agreement with a staggered conformation than with a pure eclipsed one. On the other hand, no distinction can as yet be made between *syn*(–) and *anti* conformers (or a mixture of both in exchange) with regard to Ψ. The conformational behavior of **1** may be further explored on the basis of inter-residue NOEs.[24] The key inter-residue NOEs (Figure 2) are $H3^{ax}_{sial}$–$H3_{Gal}$, $H3^{eq}_{sial}$–$H3_{Gal}$, $H3^{ax}_{sial}$–$H4_{Gal}$, $H3^{eq}_{sial}$–$H4_{Gal}$, $H8_{sial}$–$H3_{Gal}$, and $H8_{sial}$–$H4_{Gal}$. The presence of a methylene proton H_b at the pseudo-glycosidic linkage allowed us to obtain more conformational information as compared to regular *O*-glycosides. In fact, NOEs between H_b and $H2_{Gal}$/$H4_{Gal}$ or $H3^{eq}_{sial}$/$H3^{ax}_{sial}$ at the sialic ring may be expected depending on the conformation. These NOEs may allow a better description of the conformations about the pseudo-glycosidic and aglyconic linkages ϕ/Ψ. Thus, for the *anti* orientation about ψ (in principle consistent with the low $J_{Hb–H3}$ value), an intense NOE (corresponding to a distance shorter than 2.5 Å) would be expected between H_b and $H4_{Gal}$. However, any such NOE was below the limit of detection in all our experiments (either 1-D or 2-D), irrespective of the temperature or mixing time, suggesting that the average distance between these protons is greater than 3.3 Å. The absence of this H_b–$H4_{Gal}$ NOE thus rules out the existence of significant populations of rotamers about Ψ characterized by an *anti* orientation. This result restricts the conformational space available to Ψ to the *syn*(–) (minima A, C, and G) or *eclipsed* (B, D, and H) regions. With regard to the pseudo-glycosidic linkage Φ, qualitative analysis of the NOE data indicates the existence of a high degree of flexibility. Figure 1 shows (as contour levels) the Ψ/Φ values characterized by short inter-residue H–H distances superimposed on the potential energy surface calculated with AMBER* ($\varepsilon = 4 \cdot r$). It can be seen that the region characterized by short $H3^{ax}_{sial}$–$H3_{Gal}$ distances (< 3 Å) includes minima A and B [*exo-anti*/*syn*(–) and *exo-anti*/*eclipsed* conformations]. Therefore, an $H3^{ax}_{sial}$–

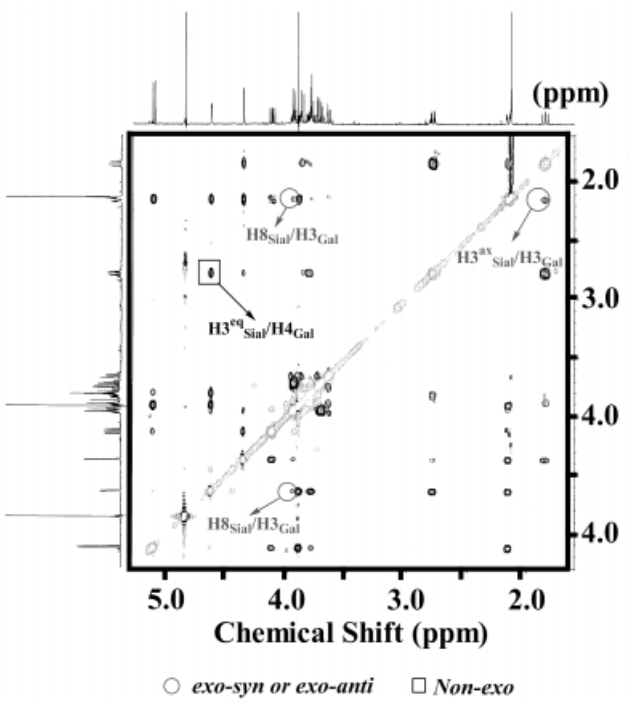

Figure 2. Part of the 2D-ROESY spectrum of **1** at 500 MHz, 303 K, D_2O, mixing time 600 ms

$H3_{Gal}$ NOE would be indicative of conformational populations around these low-energy regions. Similarly, $H3^{eq}_{sial}$–$H4_{Gal}$ and $H8_{sial}$–$H3_{Gal}$/$H8_{sial}$–$H4_{Gal}$ NOEs would be sensitive to conformational populations around minima G–H [non-*exo*/*syn*(–) and non-*exo*/*eclipsed* conformations] and C–D [*exo-syn*/*syn*(–) and *exo-syn*/*eclipsed* conformations], respectively. In fact, the observation of NOEs corresponding to the four aforementioned H–H inter-residue distances conclusively proves the presence of significant populations of conformers having the three basic staggered orientations about ϕ (*exo-syn*, *exo-anti*, and non-*exo*). Thus, qualitative analysis of the NOE/*J* data indicates that the three staggered orientations of ϕ are populated, while Ψ is restricted to the *syn*(–) and/or *eclipsed* regions (between –60 and 0°). A schematic representation of the main conformational families of **1** showing the relevant H–H inter-residue distances is given in Figure 3.

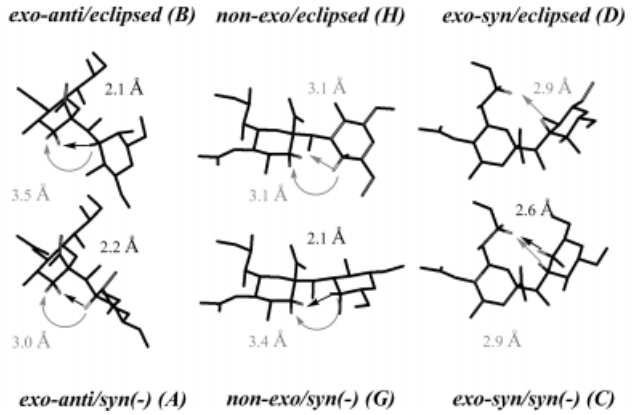

Figure 3. Simplified views of the global and local low-energy minima obtained by AMBER* calculations for compound **1**; the expected key NOEs are indicated for each conformer

To further elaborate the above conclusions, a more detailed analysis of the NMR data was carried out. Up to 13 NOEs providing conformational information on **1** could unambiguously be identified (Figure 2). The relationship between NOEs and proton–proton distances is also well-established[24] and can be delineated at least semi-quantitatively by considering a full relaxation matrix analysis. Since the NOE intensities are sensitive to the corresponding conformer populations, a first indication of the population distribution could be obtained by focusing on these key NOEs (Table 2), which are not compatible with one unique conformation. To test the validity of the theoretical MM surfaces, the NMR-spectroscopic parameters (*J* values and NOEs) of **1** were calculated from the corresponding probability distributions. No agreement between the experimental and MM-predicted *J*/NOE values was obtained. By comparing the observed with the expected NOEs, it emerged that the MM distribution, which is mainly based on *exo-anti*/*syn*(–) and *exo-syn*/*syn*(–) regions, cannot explain the presence of a strong NOE between protons $H3^{ax}_{sial}$ and $H4_{Gal}$, as well as a very weak but observable NOE between $H3^{eq}_{sial}$ and $H4_{Gal}$. In fact, it would be necessary to include some contribution from non-*exo*/*syn*(–) conformers to satisfactorily explain all the NOEs (see above).

Table 2. Experimental NOE-derived and calculated inter-residue proton–proton distances with conformational information for unconstrained MD simulations and for the best tar-MD simulation; the dielectric constant is also given

Distance	Expt. [Å]	Non-constrained $\varepsilon = 4 \cdot r$	Non-constrained $\varepsilon = 80$	MD-tar $\varepsilon = 1 \cdot r$
H3′a–H3	2.5–2.8	*2.18*	*2.28*	2.76
H3′e–H3	3.0–3.5	2.91	2.96	3.12
H3′a–H4	> 3.3	*2.38*	*2.53*	3.20
H3′e–H4	2.3–2.6	*3.94*	*2.86*	2.67
H8′–H3	2.9–3.3	*6.32*	*4.71*	3.26
H8′–H4	3.0–3.5	*4.30*	*3.72*	3.39
H3′a–Hb	2.3–2.6	*3.09*	*2.98*	2.56
H3′e–Hb	2.8–3.2	*2.63*	*2.65*	2.89
H2–Hb	2.5–2.9	*3.07*	2.99	2.75
H3–Hb	2.1–2.5	2.39	2.40	2.51
H4–Hb	> 3.3	3.81	3.80	3.83
H3′a–H2	> 3.3	4.82	4.82	4.77
H3′e–H2	> 3.3	5.28	5.20	4.97
J	Expt. (Hz)	Non-constrained $\varepsilon = 4 \cdot r$	Non-constrained $\varepsilon = 80$	MD-tar $\varepsilon = 1 \cdot r$
Hb–H3	1.9	2.22	2.30	1.83

With the conformational information corresponding to 13 NOEs and 1 *J* value at hand, to gain a quantitative insight into the equilibrium we decided to use time-averaged restrained molecular dynamics using the AMBER 5.0 package (tar-MD)[17,18] to obtain an experimentally-based overall average distribution of conformers. This methodology has rarely been used in conformational analysis of carbohydrate molecules, probably due to the lack of sufficient experimental constraints. As a first step, to determine the conformational preferences of **1** according to AMBER 5.0, two 15 ns unconstrained MD trajectories were allowed to evolve starting from different geometries and using different dielectric constant values ($\varepsilon = 4 \cdot r$ and $\varepsilon = 80$). The conformational behavior predicted by this force-field (Figure 4) was very similar to that deduced from the AMBER* potential energy surfaces, with major populations around minima A, B, C, and D. Although both trajectories correctly reproduced the experimental $J_{Hb–H3gal}$ value (Table 2), large deviations from the NMR-derived distances were observed in both cases. Clearly, a higher degree of flexibility about ϕ was required in order to reproduce the experimental distances. Thus, three MD-tar simulations of **1** were carried out using the AMBER 5.0 force field,[18] three starting geometries (minima A, C, and G), and a dielectric constant value of $1 \cdot r$. The agreement between the expected and the observed NMR-derived parameters was very satisfactory (Table 2). According to Neuhaus and Williamson:[24] "*the ability to fit NOE data using predicted conformations cannot be taken to mean that those conformations are necessarily those that are present; other choices might well fit the NOE data also*". Nevertheless, the combination of 1 *J* value and 13 observed NOEs to define just two dihedral angles gives confidence in the populations obtained; variation of these angles only modified the energy surfaces described above by leading to different minima populations. The distributions are shown in Figure 4 and the results gathered are summarized in Table 2.

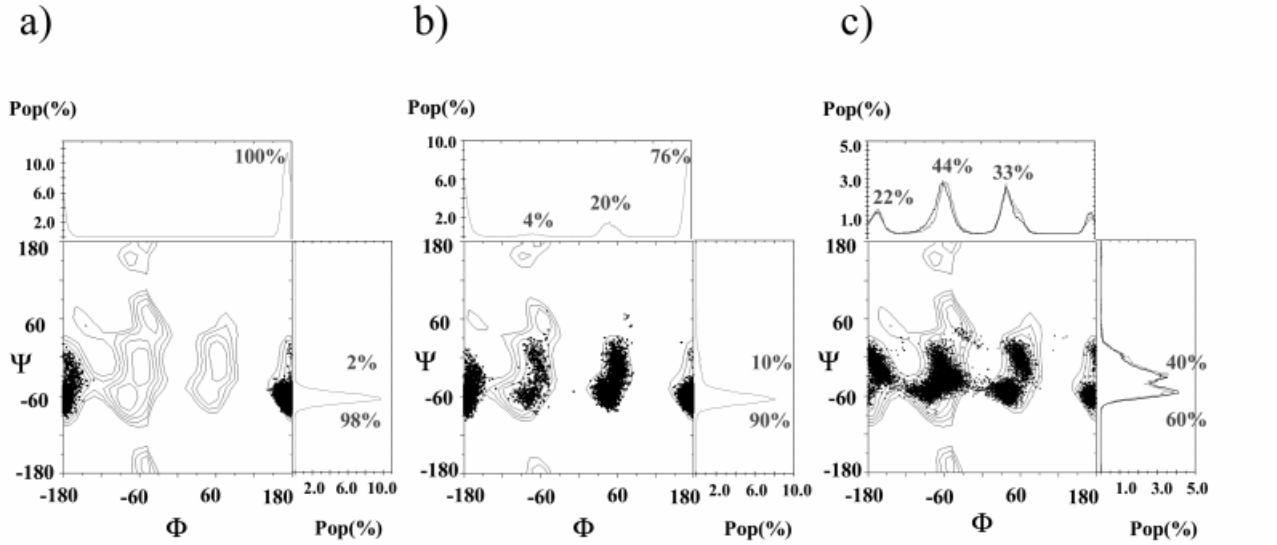

Figure 4. Trajectories corresponding to different MD simulations performed for **1**: (a) unrestrained MD simulation with $\varepsilon = 4 \cdot r$; the starting geometry corresponds to the *exo-anti/syn*(–) conformation; no transitions about Φ are observed after 15 ns; (b) unrestrained MD simulation with $\varepsilon = 80$; the starting geometry corresponds to the non-*exo/syn*(–) conformation; no quantitative match between experimental and theoretical parameters was obtained in any case; (c) tar-MD dynamics with $\varepsilon = r$; three different starting geometries were used [*exo-syn/syn*(–), *exo-anti/syn*(–), and non-*exo/syn*(–)]; 11 NMR-derived distances and 1 coupling constant were used as constraints; the trajectories for three starting geometries produced essentially the same results; in all cases, the agreement between the back-calculated NMR parameters and the observed ones was excellent; the top and right-hand traces show the percentage of populations at any given orientation

As expected, the trajectories indicate the presence of the three similarly populated, staggered Φ values in the distribution (Figure 4). All the NOE-derived distances and *J* couplings are reproduced in a quantitative manner. As regards Ψ torsion, the energy surface is predominantly extended towards the staggered *syn*(–) conformation, although a very significant contribution from minima with lower Ψ angles (20 ± 10°) is also present.

A qualitative analysis was also performed for compound **2**. The *J* values for **1** ($J_{H3Gal\text{-}Hb}$ = 1.6 Hz) and **2** ($J_{H3Gal\text{-}Hb}$ = 4.3 Hz) differ by about 2.7 Hz. Thus, from a first-order analysis, while the population of the *syn*(–) minimum is predominant for Ψ of **1**, the *eclipsed* values are predominant for **2**, probably due to *syn*-diaxial-type 1,3-interactions between the hydroxy group and the aglycon.

The conformational behavior of the *O* analogue **3** has been studied in a number of papers.[13–16] In fact, several proton–proton distances sensitive to conformer populations are present in compound **3**, which can be detected by NOE experiments.[13–16,24] Thus, various authors have reported the presence of $H3^{ax}_{Sial}$–$H3_{Gal}$, $H3^{eq}_{Sial}$–$H3_{Gal}$, $H8_{Sial}$–$H3_{Gal}$, and $H8_{Sial}$–$H4_{Gal}$ NOEs. The potential energy surface calculated for **3** using the AMBER 5.0 force field is shown in Figure 5. Glycosidic torsion angles are defined as above with C_b replaced by O. Analysis of the map for **3** shows that in this case only two low-energy regions dominate the surface (Figure 5). The main low-energy region includes the global minimum (*exo-syn/eclipsed)* and is clearly extended towards the *exo-syn/syn*(–) minimum. The second low-energy region is located around the *exo-anti/eclipsed* minimum. In contrast to the *C* analogues (**1** and **2**), for compound **3** there is no low-energy geometry characterized by a non-*exo*-anomeric orientation about ϕ. This map is in qualitative agreement with conformational descriptions reported in the literature,[13–16] although a greater population about the *exo-anti/syn*(–) and *exo-anti/eclipsed* minima would be required in order to explain the observed $H3^{ax}_{Sial}$–$H3_{Gal}$ and $H3^{eq}_{Sial}$–$H3_{Gal}$ NOEs.

Conclusions

Our results for sialyl-*O*/*C*-saccharides indicate that, in the absence of stereoelectronic stabilization, significant populations of conformers that are not consistent with the *exo*-anomeric disposition may be adopted. Consequently, **1** and **3** show different population distributions about the glycosidic Φ angle.

Experimental NMR results have demonstrated a different conformational behavior of *C*-glycoside **1** with respect to *O*-glycoside **3**. When the conformational distribution about Φ of **3** is compared with that of *C*-glycoside **1**, the *exo*-anomeric conformation can be seen to be additionally stabilized. The importance of the *exo*-anomeric effect[8] as the major factor in determining the particular conformation adopted by *O*-glycosides has been questioned.[10,11] However, our data indicate that the *exo*-anomeric effect is indeed a key factor in determining the conformational behavior about the angle Φ of *O*-glycosides in aqueous solution.

As regards the use of *C*-glycosides as *O*-glycoside isosters, it is evident that, due to the small energy differences between conformers, conformations other than the major one that are present in solution may also be bound at the binding sites of proteins. Evidently, topological features of the protein binding site and the dynamic equilibrium of the flexible *C*-glycoside will contribute to the final outcome. Furthermore, the increased flexibility of *C*-glycosides could

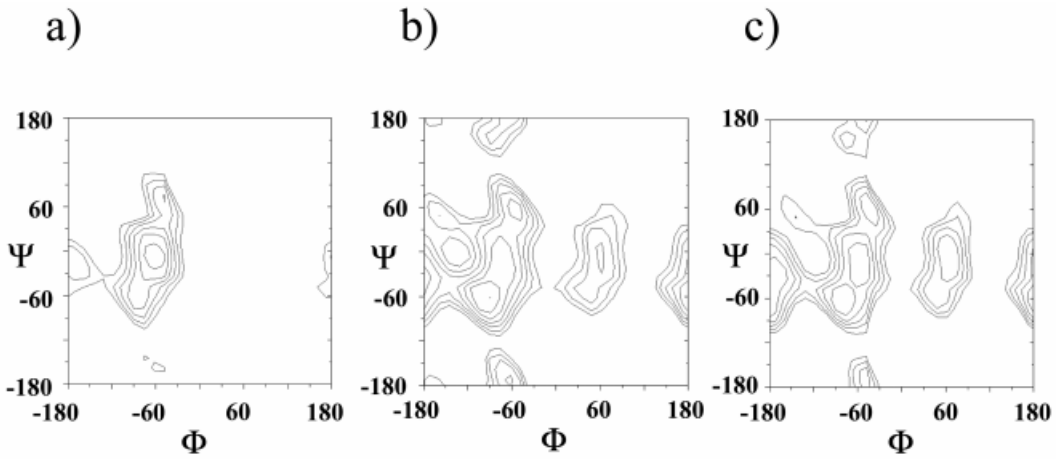

Figure 5. Steric energy maps calculated using the AMBER* force-field with $\varepsilon = 4 \cdot r$ for the natural analogue **3** (a), for a putative CH_2 analogue in order to predict the consequences of hydroxylation at the bridge (b), and for compound **1** (c); the maps for **1** and its corresponding CH_2 analogue are very similar, indicating that the R-hydroxy group plays only a minor role; in contrast, the non-*exo*-anomeric area is predicted to disappear for the natural O compound **1**, in agreement with reported results[13,14,16]

have an impact on the thermodynamic balance of the recognition process. Thus, the dissociation constants for protein–carbohydrate interactions are typically in the millimolar range, in spite of the large binding enthalpy, since the entropy changes accompanying binding restrict the impact of enthalpically favorable interactions. The observed negative entropy of binding could arise from restrictions of flexibility of the sugar and/or the protein side-chains or by reorganization of the water structure. If the restriction of ligand flexibility upon binding does indeed contribute to the negative entropy values, then a less favorable entropic balance can be expected for more flexible ligands. These results, along with those previously obtained for *C*-lactose (which has a β-glycosidic linkage) are important in the context of drug design.[7,25–27] Thus, while the flexibility of *C*-disaccharides might limit their use as therapeutic agents, these compounds are still excellent probes for studying the binding sites of proteins and enzymes,[27] as well as for assessing the conformational properties of saccharides.[7c]

Experimental Section

Compounds: The *C*-glycosyl analogues of sialyl-α-(2→3)-galactose (**1** and **2**, Scheme 1) were synthesized in their protected form[19] and then deprotected for the current study.

5-Acetamido-2,6-anhydro-3,5-dideoxy-2-*C*-{(*R*)-hydroxy-[3-(*p*-methoxyphenyl-3-deoxy-β-D-galactopyranosidyl)]methyl}-D-*erythro*-L-*manno*-nonate (1) and 5-Acetamido-2,6-anhydro-3,5-dideoxy-2-*C*-{(*S*)-hydroxy-[3-(*p*-methoxyphenyl-3-deoxy-β-D-galactopyranosidyl)]-methyl}-D-*erythro*-L-*manno*-nonate (2): To solution of **1a** and **2a** (50 mg) in 5 mL of the solvent system MeOH/EtOAc/H_2O, 4:4:2, containing 1 drop of 80% aq. HOAc solution, was added 5% Pd on activated carbon (15 mg). The flask was then closed with an H_2 balloon and the contents were vigorously stirred for 24 h at room temperature. The mixture was subsequently filtered and the filtrate was concentrated under reduced pressure. The residue was dissolved in pyridine (3 mL) and acetic anhydride (2 mL) and the resulting solution was stirred for 16 h at room temp. Concentration under reduced pressure and purification of the residue by flash column chromatography (EtOAc as eluent) gave pure **1b** and **2b** (39 mg, 88%) as a white solid. To a solution of **1a** and **2b** (36 mg) in MeOH (9 mL) was added a catalytic amount of NaOMe and the mixture was stirred overnight at room temp. Then, 0.2 M aq. KOH solution (1 mL) was added and the mixture was stirred for 8 h at room temp. It was then neutralized, desalted with 3 g of Amberlite IR-120 (H^+) exchange resin, filtered, and concentrated to furnish **1** and **2** (19 mg, 87%) as a white solid. – **1:** $[\alpha]_D^{23} = -9$ ($c = 1$, $CHCl_3$); HR-FAB-MS (+ve): calcd. for $C_{25}H_{36}NO_{15}$ [M – H]$^-$ 590.2088, found 590.2085. – **2:** $[\alpha_D]^{23} = +1$ ($c = 1$, $CHCl_3$); HR-FAB-MS (+ve): calcd. for $C_{25}H_{36}NO_{15}$ [M – H]$^-$ 520.2888; found 520.2086.

Molecular Mechanics and Dynamics Calculations: Molecular mechanics and dynamics calculations were performed with the AMBER* force-field implemented in MACROMODEL 4.5[28] as described elsewhere.[7a,12] Dielectric constants of $\varepsilon = 80$ and $4 \cdot r$ were used. – For the tar-MD simulations, compound **1** was constructed using the X-Leap program.[29] All molecular dynamics simulations were carried out using the Sander module within the AMBER 5.0 package. As a first step, two 15-ns unrestrained MD simulations were run starting from minima A [*exo-anti*/*syn*(–)] and C [non-*exo*/*syn*(–)]. Dielectric constant values of $\varepsilon = 4 \cdot r$ and 80 were used, respectively. – In addition, MD-tar simulations were carried out for **1**. NOE-derived distances were included as time-averaged distance constraints and the scalar coupling constant ($J_{Hb\text{-}H3Gal}$) as a time-averaged *J* coupling restraint. To simplify the calculation, the dihedral angles $O6_{sial}$–$C6_{sial}$–$C7_{sial}$–$C8_{sial}$ and $C6_{sial}$–$C7_{sial}$–$C8_{sial}$–$C9_{sial}$ corresponding to the sialic acid side-chain were constrained (with no time-averaging) to the –20/–100° and 160–210° ranges, respectively, in accordance with the coupling constant information. An $(r^{-6})^{-1/6}$ average was used for the distances and a linear average was used for the coupling constant. The *J* value is related to the torsion τ by the well-known Karplus relationship: $J = A\cos^2(\tau) + B\cos(\tau) + C$. Values of *A*, *B*, and *C* were chosen to fit the extended Karplus–Altona relationship.[23] At the end of the simulations, the averaged *J* value was calculated using both the regular Karplus and the complete Altona equations and compared to the experimental value. – Trial simulations were run using different simulation lengths (between 1 and 15 ns), different force constants for the distances (between 10 and 30 kcal/molÅ^2), and *J* coupling (between 0.1 and 0.3 kcal/molHz^2) constraints. Different values for the exponential decay constant (between 100 ps and 1.5 ns) were

also tested. These preliminary runs showed that for flexible molecules such as **1**, the use of exponential decay constants shorter than 1 ns produced unstable trajectories and led, in some cases, to severe distortions of the pyranose rings. In contrast, good results were obtained when using exponential decay constant values of 1 ns or longer. It has been estimated[17c] that simulation lengths about one order of magnitude greater than the exponential decay constant should be used to generate reliable estimates of average properties. Thus, the final trajectories were run using an exponential decay constant of 1.5 ns and a simulation length of 15 ns. – It is also known[17b] that when using large force constants for the *J* coupling constraints, the molecule can get trapped in high-energy, physically improbable, incorrect minima. In order to circumvent this false minima problem, low values (between 0.1 and 0.3 kcal/molHz^2) were used for the *J* coupling restraint force constants. – Three final 15-ns MD-tar simulations (starting from minima A, C, and G) were run for **1** using a dielectric constant value of $\varepsilon = 1 \cdot r$. Population distributions obtained starting from different initial geometries were almost identical, indicating that the simulation length was adequate for a proper convergence of the conformational parameters. Average distance and *J* values obtained in this way were found to correctly reproduce the experimental ones.

NMR Spectroscopy: The NMR experiments were performed with Varian Unity and Bruker DRX 500 spectrometers. 2D-NOESY and 2D-ROESY experiments were performed using the standard sequences. 1D-selective NOE spectra were acquired using the double-echo sequence proposed by Shaka and co-workers[30] at six different temperatures: 10, 15, 20, 25, 30, and 35 °C. Five different mixing times, 200, 400, 600, 800, and 1000 ms, were used. NOESY back-calculations were performed as described previously.[7a,12]

Acknowledgments

Financial support from the DGICYT (Grant PB96–0833) and the TMR-EU is gratefully acknowledged.

[1] H. J. Gabius, S. Gabius (Eds.), *Glycosciences: Status and Perspectives*, Chapman Hall, London, **1997**.

[2] [2a] J. M. Rini, *Ann. Rev. Biophys. Biomol. Struct*. **1993**, *24*, 551–577. – [2b] H.-J. Gabius, *Eur. J. Biochem*. **1997**, *243*, 543–576. – [2c] J. Hirabayashi, *Trends Glycosci. Glycotechnol*. **1997**, *9*, 1–190. – [2d] H. Kaltner, B. Stiersdorfer, *Acta Anat*. **1998**, *161*, 162–179. – [2e] J. Kopitz, C. von Reitzenstein, M. Burchert, M. Cantz, H. J. Gabius, *J. Biol. Chem.* **1998**, *273*, 11205–11211. – [2f] N. L. Perillo, M. E. Marcus, L. G. Baum, *J. Mol. Med.* **1998**, *76*, 402–412. – [2g] M. L. Philips, E. Nudelman, F. C. A. Gaeta, M. Perez, K. Singhal, S. Hakomori, J. C. Paulson, *Science* **1990**, *250*, 1132.

[3] [3a] M. D. H. Postema, *C-Glycoside Synthesis*, CRC Press, Boca Raton, **1995**. – [3b] W. Levy, D. Chang (Eds.), *Chemistry of C-Glycosides*, Elsevier, Cambridge, **1995**. – [3c] B. A. Johns, Y. T. Pan, A. D. Elbein, C. R. Johnson, *J. Am. Chem. Soc.* **1997**, *119*, 4856–4865.

[4] Y. Du, R. J. Linhardt, I. R. Vlahov, *Tetrahedron* **1998**, *54*, 9913–9959.

[5] [5a] R. V. Weatherman, L. L. Kiessling, *J. Org. Chem*. **1996**, *61*, 534. – [5b] R. V. Weatherman, K. H. Mortell, M. Chervenak, L. L. Kiessling, *Biochemistry* **1996**, *35*, 3619.

[6] K. N. Houk, J. E. Eksterowicz, Y. Wu, C. D. Fuglesang, D. R. Mitchell, *J. Am. Chem. Soc.* **1993**, *115*, 4170–4177.

[7] [7a] J. F. Espinosa, F. J. Cañada, J. L. Asensio, M. Martín-Pastor, H. Dietrich, M. Martín-Lomas, R. R. Schmidt, J. Jiménez-Barbero, *J. Am. Chem. Soc.* **1996**, *118*, 10862–10871. – [7b] G. Rubinstenn, P. Sinay, P. Berthault, *J. Phys. Chem. A* **1997**, *101*, 2536. – [7c] J. L. Asensio, A. Garcia, F. J. Cañada, M. T. Murillo, A. Fernández-Mayoralas, B. A. Johns, J. Kozak, Z. Zhu, C. R. Johnson, J. Jiménez-Barbero, *J. Am. Chem. Soc.*, in press.

[8] [8a] R. U. Lemieux, S. Koto, D. Voisin, *Am. Chem. Soc. Symp. Ser*. **1979**, *87*, 17–29. – [8b] G. R. J. Thatcher, *The Anomeric Effect and Associated Stereoelectronic Effects*, American Chemical Society, Washington DC, **1993**. – [8c] A. J. Kirby, *The Anomeric Effect and Related Stereoelectronic Effects at Oxygen*, Springer-Verlag, Heidelberg, Germany, **1983**. – [8d] H. Thogersen, R. U. Lemieux, K. Bock, B. Meyer, *Can. J. Chem.* **1982**, *60*, 44–65. – [8e] I. Tvaroska, T. Bleha, *Adv. Carbohydr. Chem. Biochem.* **1989**, *47*, 45–103. – [8f] K. B. Wiberg, M. Á. Murcko, *J. Am. Chem. Soc.* **1989**, *111*, 4821–4827. – [8g] I. Tvaroska, J. P. Carver, *J. Phys. Chem*. **1995**, *99*, 6234–6241.

[9] M. Martín-Pastor, J. F. Espinosa, J. L. Asensio, J. Jimenez-Barbero, *Carbohydr. Res.* **1997**, *298*, 15–47.

[10] [10a] A. Wei, K. M. Boy, Y. Kishi, *J. Am. Chem. Soc.* **1995**, *117*, 9432–9437. – [10b] Y. Wang, P. G. Goekjian, D. V. Ryckman, W. H. Miller, S. A. Babirad, Y. Kishi, *J. Org. Chem.* **1992**, *57*, 482–489. – [10c] T. Wu, P. G. Goekjian, Y. Kishi, *J. Org. Chem.* **1987**, *52*, 4819–4823. – [10d] A. Wei, Y. Kishi, *J. Org. Chem.* **1994**, *118*, 88–96, and references therein.

[11] R. Ravishankar, A. Surolia, M. Vijayan, S. Lim, Y. Kishi, *J. Am. Chem. Soc.* **1998**, *120*, 11297–11303.

[12] J. F. Espinosa, M. Bruix, O. Jarreton, T. Skrydstrup, J.-M. Beau, J. Jiménez-Barbero, *Chem. Eur. J.* **1999**, 442–448.

[13] [13a] J. Breg, L. M. Kroon-Batenburg, G. Strecker, J. Montreuil, J. F. G. Vliegenthart, *Eur. J. Biochem.* **1989**, *178*, 727–739. – [13b] Y. Ichikawa, Y. C. Lin, D. P. Dumas, G. J. Shen, E. Garcia-Junceda, M. A. Williams, R. Bayer, C. Ketcham, L. E. Walker, J. C. Paulson, C. H. Wong, *J. Am. Chem. Soc.* **1992**, *114*, 9283–9285. – [13c] T. J. Rutherford, D. G. Spackman, P. J. Simpson, S. W. Homans, *Glycobiology* **1994**, *5*, 59–65. – [13d] C. Mukhopadhyay, C. A. Bush, *Biopolymers* **1993**, *34*, 15–23.

[14] [14a] S. Sabesan, J. Duus, T. Fukunaga, K. Bock, S. Ludvigsen, *J. Am. Chem. Soc.* **1991**, *113*, 3236–3241. – [14b] H. C. Siebert, G. Reuter, R. Schauer, C. W. von der Lieth, J. Dabrowski, *Biochemistry* **1992**, *31*, 6962–6967. – [14c] L. Poppe, J. Dabrowski, C. W. von der Lieth, K. Koike, T. Ogawa, *Eur J. Biochem.* **1990**, *189*, 313–317.

[15] [15a] J. M. Coteron, K. Singh, J. L. Asensio, M. Dominguez-Dalda, A. Fernandez-Mayoralas, J. Jimenez-Barbero, M. Martin-Lomas, J. Abad-Rodriguez, M. Nieto-Sampedro, *J. Org. Chem.* **1995**, *60*, 1502–1519. – [15b] K. Scheffler, B. Ernst, A. Katopodis, J. L. Magnani, W. T. Wang, R. Weisemann, T. Peters, *Angew. Chem. Int. Ed. Engl.* **1995**, *34*, 1841–1844.

[16] [16a] R. Harris, G. R. Kiddle, R. A. Field, M. J. Milton, B. Ernst, J. L. Magnani, S. W. Homans, *J. Am. Chem. Soc.* **1999**, *121*, 2546–2551. – [16b] L. Poppe, G. S. Brown, J. S. Philo, P. V. Nikrad, B. H. Shah, *J. Am. Chem. Soc.* **1997**, *119*, 1727–1730.

[17] [17a] A. E. Torda, R. M. Scheek, W. F. van Gunsteren, *J. Mol. Biol.* **1990**, *214*, 223–235. – [17b] D. A. Pearlman, *J. Biomol. NMR* **1994**, *4*, 1–16. – [17c] A. E. Torda, R. M. Scheek, W. F. van Gunsteren, *Chem. Phys. Lett.* **1989**, *157*, 289–294.

[18] [18a] D. A. Pearlman, D. A. Case, J. W. Caldwell, W. S. Ross, T. E. Cheatham, S. DeBolt, D. Ferguson, G. Siebal, P. Kollman, *Comp. Phys. Commun*. **1995**, *91*, 1–41. – [18b] D. A. Pearlman, P. A. Kollman, *J. Mol. Biol*. **1991**, *220*, 457–479.

[19] H. G. Bazin, Y. Du, T. Polat, R. L. Linhardt, *J. Org. Chem.* **1999**, *64*, 7254.

[20] A general survey of conformation of carbohydrates is presented in: A. D. French, J. W. Brady, *Computer Modelling of Carbohydrate Molecules*, American Chemical Society, **1990**.

[21] [21a] B. Meyer, *Topics Curr. Chem.* **1990**, *154*, 141. – [21b] K. Bock, *Pure Appl. Chem*. **1983**, *55*, 605.

[22] [22a] A. Imberty, *Curr. Opin. Struct. Biol.* **1997**, *7*, 617–623. – [22b] T. Peters, B. M. Pinto, *Curr. Opin. Struct. Biol.* **1996**, *6*, 710–720.

[23] For the relation between H/H couplings and conformation, see: C. A. G. Haasnoot, F. A. A. M. de Leeuw, C. Altona, *Tetrahedron* **1980**, *36*, 2783.

[24] D. Neuhaus, M. P. Williamson, *The Nuclear Overhauser Effect in Structural and Conformational Analysis*, VCH Publishers, New York, **1989**.

[25] J. F. Espinosa, F. J. Cañada, J. L. Asensio, H. Dietrich, M. Martín-Lomas, R. R. Schmidt, J. Jiménez-Barbero, *Angew. Chem. Int. Ed. Engl.* **1996**, *35*, 303–306.

[26] J. F. Espinosa, E. Montero, A. Vian, J. Garcia, H. Dietrich, M. Martín-Lomas, R. R. Schmidt, A. Imberty, F. J. Cañada, J. Jiménez-Barbero, *J. Am. Chem. Soc.* **1998**, *120*, 10862–10871.

[27] J. L. Asensio, J. F. Espinosa, S. Andre, H. Dietrich, M. Martín-Lomas, R. R. Schmidt, F. J. Cañada, H.-J. Gabius, J. Jiménez-Barbero, *J. Am. Chem. Soc.* **1999**, *121*, 8995–9000.
[28] F. Mohamadi, N. G. J. Richards, W. C. Guida, R. Liskamp, C. Caufield, G. Chang, T. Hendrickson, W. C. Still, *J. Comput. Chem.* **1990**, *11*, 440–467.
[29] C. E. A. F. Schafmeister, W. S. Ross, V. Romanovski, *LEAP*, University of California, San Francisco, **1995**.
[30] K. Stott, J. Stonehouse, J. Keeler, T.-L. Hwang, A. J. Shaka, *J. Am. Chem. Soc*. **1995**, *117*, 4199.

Received October 18, 1999
[O99577]